

**Lattice thermal conductivity of cubic GeTe with vacancy defects**Minjae Ghim, Young-Jae Choi , and Seung-Hoon Jhi \**Department of Physics, Pohang University of Science and Technology, Pohang 37673, Republic of Korea*

(Received 20 December 2022; accepted 20 April 2023; published 2 May 2023)

Germanium telluride (GeTe) and its variants are promising compounds as high figure of merit thermoelectric materials due to their low lattice thermal conductivity. The strong anharmonicity and the intrinsic Ge vacancies are shown to be the origin of the low thermal conductivity. While the anharmonic effect on the lattice thermal conductivity has been systematically studied using the perturbation theory, the vacancy disorder has been treated perturbatively mostly as an extreme case of phonon-isotope scattering. This simplification ignores realistic features such as the nonbonding character and the detailed local environments near the vacancies. In this study, we calculate the lattice thermal conductivity of the cubic GeTe by considering the anharmonicity and the vacancy disorder on the same footing using the machine-learning potential molecular dynamics. We obtain the spectral function via the nonperturbative approaches, the velocity autocorrelation function, and the phonon unfolding scheme to investigate the effect of the vacancies on the lattice thermal conductivity. We find that the reduction in the lattice thermal conductivity by the vacancies originates from the momentum-dependent scattering of the acoustic phonon modes and the momentum-independent scattering of the optical phonon modes as determined by the strength of the anharmonicity.

DOI: [10.1103/PhysRevB.107.184301](https://doi.org/10.1103/PhysRevB.107.184301)**I. INTRODUCTION**

Lattice thermal conductivity of solids is a key measure that determines the heat transport and thermal properties of the materials. Yet its calculation with an accuracy of *ab initio* methods is very complex and computationally demanding when the materials are disordered or contain defects as it is governed by both intrinsic and extrinsic effects. Germanium telluride (GeTe) is a narrow-gap semiconductor with low lattice thermal conductivity and shows a sizable thermoelectric figure of merit in the intermediate temperature range of 600–800 K [1]. Introducing defects, nanostructures [2–6], or elemental dopants [7–10] further enhances the figure of merit by reducing the lattice thermal conductivity. GeTe and its variants have thus been considered as an alternative to toxic PbTe-based thermoelectric materials.

The strong three-phonon anharmonicity is the primary origin of the low lattice thermal conductivity of the rhombohedral GeTe ( $\alpha$ -GeTe). The lowest-order perturbation theory that includes only the three-phonon processes reproduces the measurement of the lattice thermal conductivity of  $\alpha$ -GeTe [11]. On the other hand, the origin of the low lattice thermal conductivity of the cubic phase GeTe ( $\beta$ -GeTe), the high-temperature counter part of  $\alpha$ -GeTe, is unclear even though it has a high-symmetric structure. The four-phonon processes [12] and the intrinsic Ge vacancies [11] have been considered as major sources for the low lattice thermal conductivity of  $\beta$ -GeTe.

The anharmonic effects on the lattice thermal conductivity can be systematically assessed order by order using the

perturbation theory. However, it is challenging to treat the phonon scattering by vacancies in the perturbative approach because the vacancies are more than just point defects; the formation of the vacancies not only reduces locally the atomic masses but also modifies nonlocally the interatomic force constants. Meanwhile, the vacancy is assumed as a point defect and even further simplified as a virtual isotope with mass variance  $\Delta M = 3M$  ( $M$  is the mass of a missing atom) according to the virial theorem [13]. This approximation reduces significantly the computational load of calculating the vacancy-phonon scattering but ignores the realistic features of the vacancies, such as the nonbonding character and the detailed local environments near the vacancies. The nonbonding character introduces the drastic change of the interatomic force constants depending on the atomic configurations, resulting in serious overestimation of the lattice thermal conductivity [14].

Here we investigate the lattice thermal conductivity of  $\beta$ -GeTe with vacancy defects nonperturbatively using molecular dynamics (MD). We construct the neural network potential (NNP) with the training datasets obtained from the density functional theory calculations to achieve the accuracy of *ab initio* MD (AIMD) in large systems. To clarify the effect of vacancies on the thermal conductivity, we also calculate the spectral functions of phonon in the momentum space also using the nonperturbative schemes.

**II. METHODS****A. Construction of machine learning potential**

We employed the equivariant graph neural network to construct the machine learning potential implemented in Neural

\*jhih@postech.ac.kr

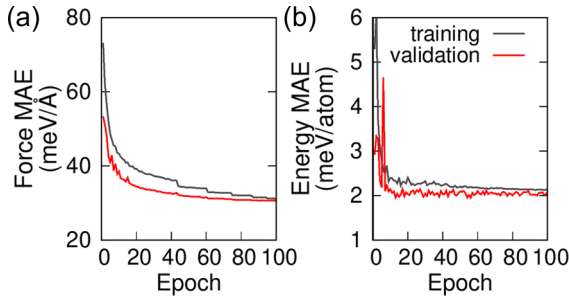


FIG. 1. Learning curves for the neural network potentials with the mean absolute error (MAE) vs the number of epochs for (a) the force and (b) the total energy.

Equivariant Interatomic Potential (NequIP) package [15]. The equivariance of the neural network tensors reflects properly the equivariance of the atomic forces and the atomic position vectors, which must be equally transformed under E(3)-group transformations. These features guarantee the interatomic potential and the corresponding forces to be trained in a systematic way, enabling reliable long-time molecular dynamics simulations. The spherical harmonics  $Y_m^l$  are adopted as the basis for the rotation-equivariant convolutional filters, and the maximum of the angular momentum index  $l$ , i.e.,  $l_{\max}$ , governs the number of the basis functions and the accuracy of the training. We used  $l_{\max} = 1$  by virtue of its cost-effectiveness as discussed in Ref. [15].

We generated a training dataset in a hybrid form combining the random sampling and subsequent atomic relaxation, namely randomized atomic-system generator (RAG) [16] as follows; first, we prepared a  $2 \times 2 \times 2$  periodic supercell of FCC conventional cell of  $\beta$ -GeTe with the experimental lattice constant of  $a = 6.015 \text{ \AA}$  at 700 K [17]. Next, we introduced Ge vacancies up to two in the periodic supercell. There are seven irreducible backbone structures, one without vacancy, one with one vacancy, and five with two vacancies. For each backbone structure, we displaced randomly the atomic positions within the maximum displacement  $\Delta_{\max} = 0.06, 0.15, 0.30, 0.60, 1.20 \text{ \AA}$  and changed the lattice constants within the maximum strain of 3% to sample the potential energy surface. In addition, we permuted randomly Ge and Te atoms. Lastly, we performed structural relaxation by force minimization of 20 steps for each randomly generated structure to scan the local energy minima. The total energy and atomic forces obtained during the relaxation for each structural configuration constitute the training dataset of 16 000 configurations in total, among which we used 15 200 configurations for training and other 800 configurations for validation. We found that 16 000 configurations are sufficient for constructing and training the potentials due to efficient schemes of NequIP and RAG methods. The neural network potentials are constructed by training the dataset with the mean absolute error (MAE) of 2.1 meV/atom for the total energy and 30.5 meV/Å for the force (Fig. 1).

### B. Estimation of the lattice thermal conductivity

The reversed nonequilibrium MD (RNEMD) [18] is exploited to calculate the lattice thermal conductivity ( $\kappa$ ). In this

scheme, the heat flow  $J_z$  is artificially generated by exchanging two atoms of the same element, one the fastest atom with  $v_{c,\max}$  in the cold sink at  $z = 0$  and  $L_z$ , and the other is the slowest atom with  $v_{h,\min}$  in the hot sink at  $z = L_z/2$ , where  $L_z$  is the supercell size along the  $z$  direction. As a result, the temperature gradient  $\partial T/\partial z$  is induced between the cold and heat sinks. Then,  $\kappa$  can be expressed as

$$\kappa = \frac{J_z}{\langle \partial T / \partial z \rangle} = \frac{1}{\langle \partial T / \partial z \rangle_L + \langle \partial T / \partial z \rangle_R} \times \sum_{\text{transfers}} \frac{mv_{c,\max}^2 - mv_{h,\min}^2}{2L_x L_y \Delta t},$$

where  $\Delta t$  the simulation time,  $L_x$  ( $L_y$ ) the periodic supercell size along the  $x$  ( $y$ ) direction, and  $m$  is the mass of the exchanged atoms. We took the linear region of the temperature distribution to estimate the temperature gradient of the left (L) side ( $0 < z < L_z/2$ ) and the right (R) side ( $L_z/2 < z < L_z$ ). We used the  $4 \times 4 \times 4N_z$  supercell ( $N_z = 5 \sim 10$ ) of the conventional cell, i.e.,  $L_x = L_y = 24.12 \text{ \AA}$  and  $L_z = 24.12 \times N_z \text{ \AA}$ .

To emulate the randomly distributed vacancies, we applied the special quasirandom structure (SQS) scheme [19] to the  $4 \times 4 \times 4$  supercell of the conventional cell with 8, 16, 24, 32 Ge vacancies (i.e., 1/32, 2/32, 3/32, 4/32 of vacancy concentrations). We subsequently expanded the SQS structure  $N_z$ -fold ( $N_z = 5 \sim 10$ ) along the  $z$  direction. We also estimated the lattice thermal conductivity of  $\beta$ -GeTe with the uniformly ordered vacancies at concentration of 1/32, 2/32, and 4/32 in the periodic unit cell of  $(6.015 \text{ \AA}) \times (6.015 \text{ \AA}) \times (6.015 \text{ \AA})$ .

### C. Spectral function

We calculated the phonon spectral function using the velocity autocorrelation function [20] extracted from the equilibrium MD (EMD) simulation at 700 K,

$$\langle V_{\mathbf{q}}(0)V_{\mathbf{q}}(t) \rangle = \lim_{\tau \rightarrow \infty} \frac{1}{\tau} \int_0^{\tau} V_{\mathbf{q}}(t')V_{\mathbf{q}}(t'+t)dt',$$

where  $V_{\mathbf{q}}(t) = \sum_{I=1}^N \sqrt{M_I} v_I(t) e^{i\mathbf{q} \cdot \mathbf{R}_I}$ . Applying the Fourier transformation, the  $q$ -resolved spectral function can be obtained

$$G_{\mathbf{q}}(\omega) = \int_{-\infty}^{\infty} \langle V_{\mathbf{q}}(0)V_{\mathbf{q}}(\tau) \rangle e^{i\omega\tau} d\tau.$$

The spectral function is decomposed into the mode-dependent spectral function  $G_{\mathbf{q}}(\omega) = \sum_s G_{qs}(\omega)$ , where  $G_{qs}(\omega) = \int_{-\infty}^{\infty} \langle v_{qs}(0)v_{qs}(\tau) \rangle e^{i\omega\tau} d\tau$  and  $v_{qs}(t) = \mathbf{V}_{\mathbf{q}}(t) \cdot \epsilon_{qs}$  [21]. We can define the mode-dependent spectral function of the systems with vacancy defects using  $\epsilon_{qs}$  of the pristine  $\beta$ -GeTe and treating the vacancies as immobile atoms with  $v_I(t) = 0$ .

For EMD simulation, we used a  $16 \times 16 \times 16$  supercell of the primitive cell. To emulate the randomly distributed vacancies, we constructed SQS structures from the  $8 \times 8 \times 8$  supercell of the primitive cell that contains 16, 32, 48, and 64 Ge vacancies (vacancy concentration of 1/32, 2/32, 3/32, and 4/32 the same as in the RNEMD simulation), and then

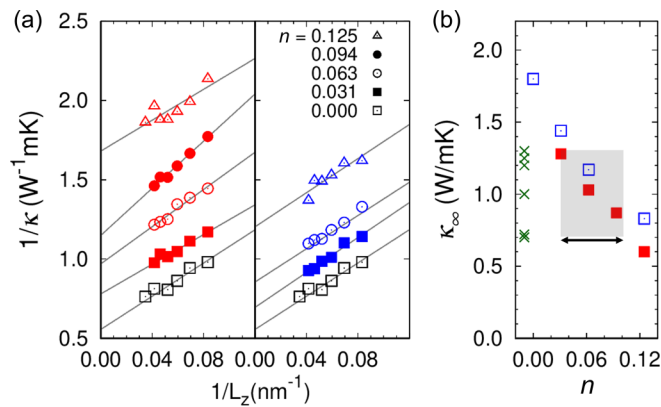


FIG. 2. Lattice thermal conductivity  $\kappa$  of  $\beta\text{-Ge}_{1-n}\text{Te}$  at 700 K (a)  $1/\kappa$  vs  $1/L_z$  for random (left panel) and ordered vacancies (right panel). The straight lines are the linear fit. (b) The bulk thermal conductivity  $\kappa_\infty$  vs the vacancy concentration  $n$ . Random (red filled square) and ordered vacancies (blue empty square). The green crosses at  $n = 0$  are measurements from Refs. [7,29–33] that did not specify the vacancy concentrations. The arrow marks the range of the intrinsic vacancy concentration ( $n = 0.03$ – $0.10$ ) from Refs. [26–28]. The shaded region highlights the range of  $n$  and  $\kappa_\infty$  in experiment.

expanded the SQS structure twofold along each primitive cell vector ( $2 \times 2 \times 2$ ).

#### D. Code availability

We exploited the LAMMPS package [22] for RNEMD and EMD simulations, UPHO code [23] for phonon unfolding, DYNAPHOPY [24] for the temperature-dependent phonon dispersion and the velocity autocorrelation function, and corresponding spectral functions.

### III. RESULTS AND DISCUSSION

Our calculated lattice thermal conductivity  $\kappa$  of  $\beta\text{-GeTe}$  at 700 K is shown in Fig. 2(a) in terms of the system size  $L_z$  and the Ge vacancy concentration  $n$ .  $1/\kappa$  is approximately expressed as [25]  $\frac{\kappa_\infty}{\kappa} = 1 + \frac{l_\infty}{L_z}$ , where  $\kappa_\infty$  is the bulk lattice thermal conductivity and  $l_\infty$  is the average mean-free path in the infinite system. High-order terms of  $l_\infty/L_z$  are ignored since  $L_z$  ( $> 12$  nm) is large enough compared to  $l_\infty$  ( $\sim 5$  nm) [12], and we obtain  $\kappa_\infty$  from the linear extrapolation of  $1/\kappa$ . For the vacancy concentration  $n = 0.03 \sim 0.10$  reported in measurement [26–28], our estimated  $\kappa_\infty$  of about 0.75–1.25  $\text{W/mK}$  [Fig. 2(b) random vacancies] is in good agreement with the measured values of 0.7–1.3  $\text{W/mK}$  [7,29–33]. Moreover,  $\kappa_\infty$  decreases as the vacancy concentration is increased, going below 1.0  $\text{W/mK}$  for  $n > 0.06$  almost half the value of pristine  $\beta\text{-GeTe}$ . This result clearly indicates that Ge vacancies affects  $\kappa_\infty$  more dominantly than the anharmonicity as gauged by the Matthiessen’s rule,  $1/\kappa_\infty = 1/\kappa_{\text{anhar}} + 1/\kappa_{\text{imp}}$  with  $\kappa_{\text{anhar}}$  and  $\kappa_{\text{imp}}$  being the anharmonicity and impurity contribution to  $\kappa_\infty$ , respectively. We note that the ordering of the vacancies can change  $\kappa_\infty$  by about 15–20% in  $\beta\text{-GeTe}$ .

Figure 3 shows calculated total spectral function, which provides the broadening of the quasiparticle peaks by the anharmonic scattering and the vacancy-phonon interaction.

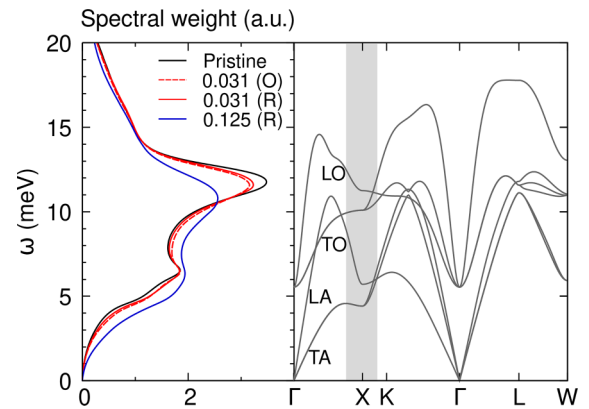


FIG. 3. (Left panel) The total spectral function of  $\beta\text{-Ge}_{1-n}\text{Te}$  ( $n = 0, 0.031, 0.125$ ) at 700 K with ordered (O) or random (R) vacancies. (Right panel) The phonon dispersion of the pristine GeTe at 700 K obtained using the temperature-dependent effective potential (TDEP) scheme. The shaded region highlights the partly dispersionless branches near the X point.

Two peaks near 6 and 12 meV develop clearly in the spectral function, corresponding to the flatlike branches near X point in the phonon dispersion. As the vacancy concentration is increased, each peak is broadened by the increase of the scattering rate. The lattice thermal conductivity, which is inversely proportional to the linewidth, is reduced accordingly. Interestingly, both peaks become slightly broader for the ordered vacancies than for the random vacancies, in shear contrast to the smaller lattice thermal conductivity for the random case. For a high vacancy concentration  $n = 0.125$ , the peaks are broadened and shifted down compared to those for  $n = 0.031$ , which indicates a reduction in the group velocity of phonons and thus the low lattice thermal conductivity. However, it is hard to distinguish the frequency shift of individual modes from the broadening of other modes.

For more detailed analysis of the individual quasiparticle peaks, we decomposed the total spectral function into the momentum  $q$ -resolved spectral function (Fig. 4) and the mode-dependent spectral function at some selected  $q$  points (Fig. 5). At low vacancy concentration  $n = 0.031$ , the quasiparticle peaks are broadened overall except for the acoustic phonon modes near  $\Gamma$  point below 3 meV [Fig. 4(c)]. The smearing of LA, TA, and TO modes near the X point (Fig. 5) is consistent with the broadening of the peaks in the total spectral function as discussed above. In addition to the broadening, the quasiparticle peaks are also shifted. The acoustic phonon modes near the  $\Gamma$  point show a downshift in frequency by at least 3%, which reduces the average group velocity and thus the thermal conductivity. The LO modes near  $\Gamma$  point also show softening, whereas the TO modes show hardening. As a result, the overall shape of the optical modes becomes less dispersive, reflecting the localization of phonon modes due to the vacancies.

It is interesting to find that the spectral function for the ordered vacancy [Fig. 4(b)] is similar to that for the random vacancy [Fig. 4(c)] at most phonon modes. However, for some acoustic phonon modes, the satellite peaks develop at about 4  $\sim$  5 meV, which reflects the splitting of quasiparticle

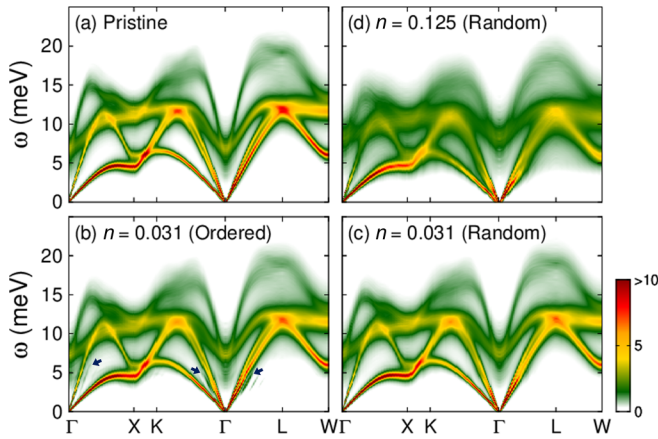


FIG. 4. Momentum  $q$ -resolved phonon spectral functions of  $\beta$ -GeTe at 700 K (a) without vacancies, (b) with the ordered vacancies, and (c), (d) with the random vacancies. The blue arrows in (b) highlight the satellite branches. The color bar indicates the spectral weights (arbitrary units).

peaks by the ordered vacancy instead of the broadening. The ordered vacancies introduce another periodicity in the lattice while breaking partly the original translational symmetry. As a result, the phonon modes at momentum  $q_1$  can hybridize with other modes at  $q_2 = \pi/c + q_1$  with  $c$  being the periodicity of the ordered vacancies. This hybridization at discrete points produces the satellite phonon peaks separated from the original peaks [Fig. 5(b)]. These satellite branches are mostly faded out by strong anharmonicity at elevated temperature  $\sim 700$  K, and only satellite peaks near the acoustic phonon modes survive [Fig. 4(b)]. On the other hand, the random vacancy breaks fully the translational symmetry, allowing the hybridization without any momentum restriction that produces the continuous broadening of the spectral function.

The linewidth of the TA modes at  $q = 3/8 L$  is about twice for the random vacancy that for the ordered vacancy (Fig. 5).

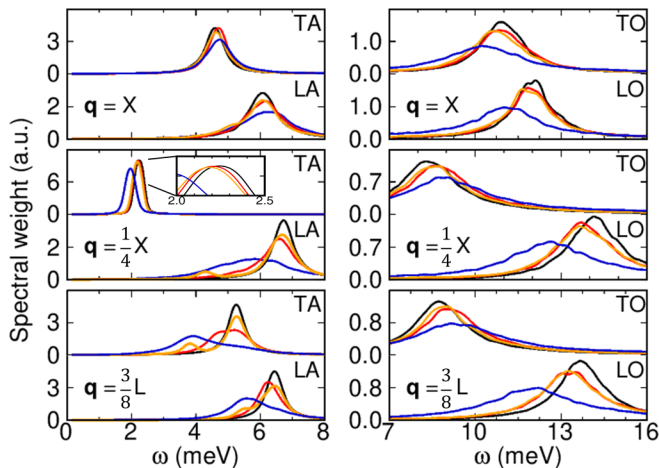


FIG. 5. Mode-dependent spectral functions at 700 K of individual branches at three characteristic  $q$  points without vacancy (black), with random vacancies  $n = 0.031$  (red), ordered vacancies  $n = 0.031$  (orange), and random vacancies  $n = 0.125$  (navy). The inset ( $q = 1/4 X$ , TA) is a magnified spectral function near  $\sim 2$  meV.

In addition, the TO modes near the  $\Gamma$  point ( $q = 1/4 X$  and  $3/8 L$ ) have a broader linewidth by about 15% for random vacancies than for ordered vacancies. This difference must be the origin of the low lattice thermal conductivity of  $\beta$ -GeTe with the random vacancy compared to that with the ordered vacancy.

A distinctive change in the spectral function occurs when the vacancy concentration is increased to  $n = 0.125$  [Fig. 4(d)]. The linewidth of the quasiparticle peaks above 5 meV increases by  $\sim 50\%$  for the random vacancies, and the peak position in frequency changes by about 20%. The spectral weights and the density of states of the phonon modes are also reduced overall due to the missing of Ge atoms. These features add up to the low lattice thermal conductivity for  $n = 0.125$ .

Finally, we calculated the harmonic spectral functions (Fig. 6) to compare the effect of the vacancies and the anharmonicity on the lattice thermal conductivity. The harmonic spectral functions are obtained by applying the unfolding scheme to the harmonic phonon dispersions in the folded Brillouin zone of the supercell with vacancies. This analysis reveals that the characteristic features of the original spectral functions (Figs. 4 and 5) come from the change in the harmonic force constants. The harmonic spectral function is split and fragmented for the ordered vacancies [Fig. 6(b)] whereas it is mostly broadened for the random vacancies [Figs. 6(c) and 6(d)]. From this finding, the satellite quasiparticle peaks of some acoustic modes near 5 meV [Fig. 4(b)] are identified originating from the splitting at  $q = 1/4 X$  and  $3/8 L$  in the harmonic spectral function for the ordered vacancies. Although the splitting occurs for other phonon modes in the harmonic spectral function, it is faded out by the anharmonicity in the original spectral function. Also, the difference between the ordered and random vacancies is obliterated as discussed above. The harmonic spectral function exhibits the mode-dependent splitting or the broadening. We observe a large splitting and also smearing in the quasiparticle peaks of the TO phonon modes near the X point, which is mapped to  $X/2$  point in the Brillouin zone of  $2 \times 2 \times 2$  conventional supercell. The flatlike dispersion from  $X/2$  to X point makes the quasiparticle peaks at the  $X/2$  and the X points overlap. In addition, the TO modes near the X point come almost from Ge atom vibrational modes [Fig. 6(a)], which interact with Ge vacancies stronger than the Te vibrational modes.

To compare directly the harmonic spectral function with the original spectral function in Fig. 4, we shifted the harmonic spectral functions by adding the same amount as the anharmonic shift of the phonon dispersion of the pristine  $\beta$ -GeTe [upper and lower panels of Figs. 6(b)–6(d) for harmonic spectral function without and with the anharmonic shift, respectively]. At first, we obtain the renormalized dynamical matrix due to the anharmonicity at 700 K in the pristine  $\beta$ -GeTe. Next, by extracting the harmonic dynamical matrix from the renormalized dynamical matrix, we obtain the anharmonic contribution to the dynamical matrix for the pristine case, namely, the anharmonic dynamical matrix. Then, we add the anharmonic dynamical matrix to the harmonic dynamical matrix with the vacancies (the matrix elements for the vacancy sites are dropped). Finally, we apply the phonon unfolding scheme to the shifted dynamical matrix. As a trade-off, the

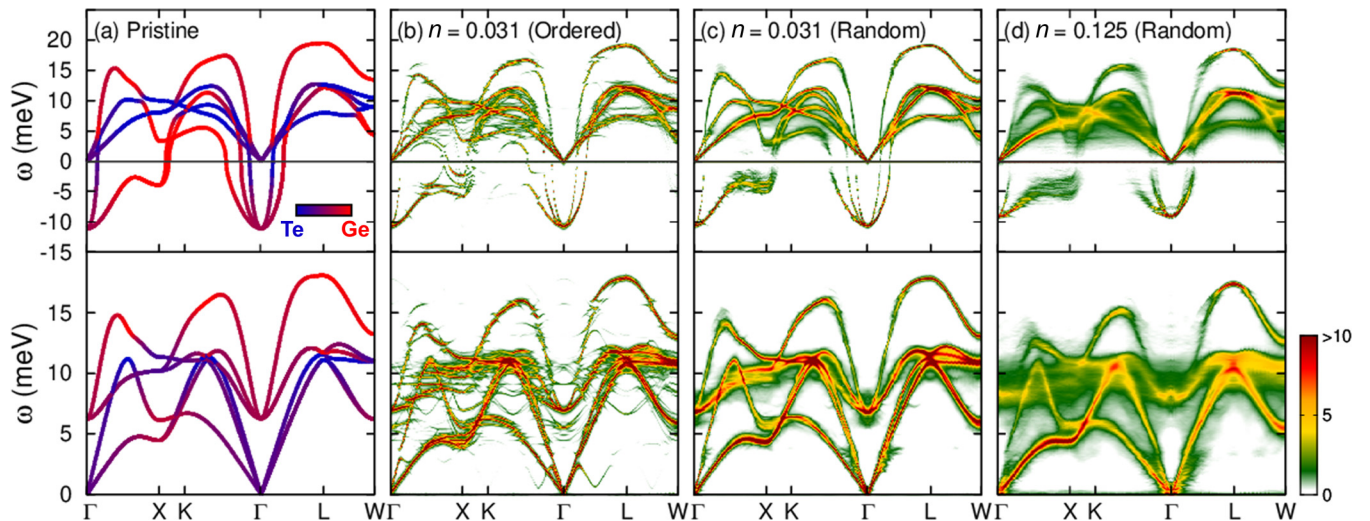


FIG. 6. (a) The harmonic phonon dispersion of the pristine  $\beta$ -GeTe at 0 K (upper panel) and 700 K (lower panel). The color indicates the atomic contribution. (b)–(d) The harmonic spectral function of  $\beta$ -GeTe with vacancies, obtained by unfolding the harmonic phonon dispersion at 0 K (upper panel) and 700 K (lower panel). The color bar indicates the spectral weights (arbitrary units).

acoustic modes near the  $\Gamma$  point show an unphysical feature. Sizable splitting or broadening occur despite their long wavelength because the shifted dynamical matrix violates largely the acoustic sum rule. Nevertheless, we expect that this unphysical noise is insignificant for high-frequency optical modes.

The quasiparticle peaks of the optical modes near the  $\Gamma$  point are clearly split [lower panel of Fig. 6(b) for ordered vacancy] or broadened [lower panel of Figs. 6(c) and 6(d) for random vacancy]. This is due to the scattering of the optical modes to other phonon modes at 7–8 meV enabled by large anharmonic shift. Similar to the optical modes near the  $\Gamma$  point, the TO modes near the X point also show a large frequency shift due to the anharmonicity. Interestingly, the splitting and the broadening of the TO modes near the X point are still sizable despite that they are Te-dominant vibrational modes. We found that the interatomic force constant between Ge and the nearest Te is much larger in effective harmonic potential at 700 K ( $\sim 0.60$  eV/Å<sup>2</sup>) than in the harmonic potential at 0 K ( $\sim 0.18$  eV/Å<sup>2</sup>). This feature explains that Te-dominant TO modes are highly affected by Ge vacancies at 700 K.

On the other hand, the LO modes along  $\Gamma$ -X have a small linewidth by the vacancies [lower panel of Figs. 6(c) and 6(d)]. Also, the large mode-dependent scattering feature of the harmonic spectral function persists in the effective harmonic spectral function that includes the anharmonic shift. We note that the original spectral functions (Figs. 4 and 5) show weak mode dependence, especially for the optical modes. In other words, the broadening of the quasiparticle peaks is similar among the optical modes in the original spectral functions. This result indicates a sizable second-order process that the optical phonon modes are scattered by both the vacancies and the anharmonicity as discussed in Ref. [34].

At the concentration  $n = 0.125$  of random vacancy [lower panel of Fig. 6(d)], the phonon dispersion shows less dispersive than the pristine case, which is consistent with the frequency shifts in the original spectral function [Fig. 4(d)].

Therefore, the quasiparticle peak shift almost comes from the change in the harmonic force constants under the vacancies.

Summarizing the above analysis, we found two significant modifications in the phonon spectral function of  $\beta$ -GeTe by the vacancies. First, some acoustic phonon modes exhibit distinctive splitting or broadening of the quasiparticle peaks, which indicates strong momentum and mode-dependent scattering of the acoustic phonon modes by the vacancies. This modification is highly sensitive to the vacancy distribution or local environments of atoms. The change in the harmonic force constants governs such a modification in the acoustic phonon modes. As temperature is increased, the effect of the vacancy ordering is washed out by the anharmonicity. Still our calculations show that some acoustic modes retain this feature of the vacancy ordering and contribute to the thermal conductivity differently. Second, the optical phonon modes show overall shift and broadening of the quasiparticle peaks due to the vacancies, representing the weak momentum dependence of the change in scattering rate. This result may be attributed to the second-order or higher-order scattering by the vacancies through the strong anharmonicity of the optical modes. These two features in combination should be the major origin of the reduction in lattice thermal conductivity by the vacancies.

#### IV. CONCLUSION

We calculated the lattice thermal conductivity of cubic GeTe using the machine-learned potential molecular dynamics considering the anharmonic scattering and the vacancy-phonon interaction on the same footing. Our calculated lattice thermal conductivity at 700 K is in good agreement with experiment. We analyzed the role of the vacancies on the low lattice thermal conductivity of cubic GeTe by calculating the spectral function nonperturbatively, the velocity autocorrelation function, and the unfolded phonon dispersion. We discovered that the reduction in the lattice thermal conductivity by the vacancies originates from

the momentum-dependent scattering of the acoustic phonon modes and the momentum-independent scattering of the optical phonon modes as determined by the strength of the anharmonicity of each phonon mode. Our analysis can be utilized to understanding the thermal conduction of defected GeTe and to its thermoelectric applications. Our approach provides a framework for consistent and quantitative analysis of the lattice dynamics and transport of disordered systems with both sizable defects and anharmonicity with an accuracy of first-principles calculations.

## ACKNOWLEDGMENTS

This study was supported by the National Research Foundation of Korea (NRF), Grant No. 2022R1A2C1006530 funded by the Korea government (MSIT), and by Samsung Electronics Co., Ltd, Grant No. IO201214-08146-01. Supercomputing resources including technical support was provided by Supercomputing Center, Korea Institute of Science and Technology Information (Contract No. KSC-2021-CRE-0534).

- [1] S. Perumal, S. Roychowdhury, and K. Biswas, High-performance thermoelectric materials and devices based on GeTe, *J. Mater. Chem. C* **4**, 7520 (2016).
- [2] Y. Gelbstein, J. Davidow, S. N. Girard, D. Y. Chung, and M. Kanatzidis, Controlling metallurgical phase separation reactions of the Ge<sub>0.87</sub>Pb<sub>0.13</sub>Te alloy for high thermoelectric performance, *Adv. Energy Mater.* **3**, 815 (2013).
- [3] Y. Gelbstein and J. Davidow, Highly efficient functional Ge<sub>x</sub>Pb<sub>1-x</sub>Te based thermoelectric alloys, *Phys. Chem. Chem. Phys.* **16**, 20120 (2014).
- [4] F. Fahrnbauer, D. Souchay, G. Wagner, and O. Oeckler, High thermoelectric figure of merit values of germanium antimony tellurides with kinetically stable cobalt germanide precipitates, *J. Am. Chem. Soc.* **137**, 12633 (2015).
- [5] S. Perumal, S. Roychowdhury, and K. Biswas, Reduction of thermal conductivity through nanostructuring enhances the thermoelectric figure of merit in Ge<sub>1-x</sub>Bi<sub>x</sub>Te, *Inorg. Chem. Front.* **3**, 125 (2016).
- [6] B. Srinivasan, C. Boussard-Pledel, and B. Bureau, Thermoelectric performance of codoped (Bi, In)-GeTe and (Ag, In, Sb)-SnTe materials processed by spark plasma sintering, *Mater. Lett.* **230**, 191 (2018).
- [7] S. Perumal, S. Roychowdhury, D. S. Negi, R. Datta, and K. Biswas, High thermoelectric performance and enhanced mechanical stability of p-type Ge<sub>1-x</sub>Sb<sub>x</sub>Te, *Chem. Mater.* **27**, 7171 (2015).
- [8] Z. Zheng, X. Su, R. Deng, C. Stoumpos, H. Xie, W. Liu, Y. Yan, S. Hao, C. Uher, C. Wolverton *et al.*, Rhombohedral to cubic conversion of GeTe via MnTe alloying leads to ultralow thermal conductivity, electronic band convergence, and high thermoelectric performance, *J. Am. Chem. Soc.* **140**, 2673 (2018).
- [9] L. Wu, X. Li, S. Wang, T. Zhang, J. Yang, W. Zhang, L. Chen, and J. Yang, Resonant level-induced high thermoelectric response in indium-doped GeTe, *NPG Asia Mater.* **9**, e343 (2017).
- [10] J. Li, X. Zhang, S. Lin, Z. Chen, and Y. Pei, Realizing the high thermoelectric performance of GeTe by Sb-doping and Se-alloying, *Chem. Mater.* **29**, 605 (2017).
- [11] Đ. Dangić, O. Hellman, S. Fahy *et al.*, The origin of the lattice thermal conductivity enhancement at the ferroelectric phase transition in GeTe, *npj Comput. Mater.* **7**, 57 (2021).
- [12] Y. Xia and M. K. Y. Chan, Anharmonic stabilization and lattice heat transport in rocksalt  $\beta$ -GeTe, *Appl. Phys. Lett.* **113**, 193902 (2018).
- [13] C. A. Ratsifaritana and P. G. Klemens, Scattering of phonons by vacancies, *Int. J. Thermophys.* **8**, 737 (1987).
- [14] N. A. Katcho, J. Carrete, Wu Li, and N. Mingo, Effect of nitrogen and vacancy defects on the thermal conductivity of diamond: An *ab initio* Green's function approach, *Phys. Rev. B* **90**, 094117 (2014).
- [15] S. Batzner, A. Musaelian, L. Sun *et al.*, E(3)-equivariant graph neural networks for data-efficient and accurate interatomic potentials, *Nat. Commun.* **13**, 2453 (2022).
- [16] Y. Choi and S. Jhi, Efficient training of machine-learning potentials by randomized atomic-system generator, *J. Phys. Chem. B* **124**, 8704 (2020).
- [17] E. M. Levin, M. F. Besser, and R. Hanus, Electronic and thermal transport in GeTe: A versatile base for thermoelectric materials, *J. Appl. Phys.* **114**, 083713 (2013).
- [18] F. Müller-Plathe, A simple nonequilibrium molecular dynamics method for calculating the thermal conductivity, *J. Chem. Phys.* **106**, 6082 (1997).
- [19] A. Zunger, S.-H. Wei, L. G. Ferreira, and J. E. Bernard, Special Quasirandom Structures, *Phys. Rev. Lett.* **65**, 353 (1990).
- [20] C. Z. Wang, C. T. Chan, and K. M. Ho, Tight-binding molecular-dynamics study of phonon anharmonic effects in silicon and diamond, *Phys. Rev. B* **42**, 11276 (1990).
- [21] D.-B. Zhang, T. Sun, and R. M. Wentzcovitch, Phonon Quasiparticles and Anharmonic Free Energy in Complex Systems, *Phys. Rev. Lett.* **112**, 058501 (2014).
- [22] S. Plimpton, Fast parallel algorithms for short-range molecular dynamics, *J. Comput. Phys.* **117**, 1 (1995).
- [23] Y. Ikeda, A. Carreras, A. Seko, A. Togo, and I. Tanaka, Mode decomposition based on crystallographic symmetry in the band-unfolding method, *Phys. Rev. B* **95**, 024305 (2017).
- [24] A. Carreras, A. Togo, and I. Tanaka, DynaPhoPy: A code for extracting phonon quasiparticles from molecular dynamics simulations, *Comp. Phys. Comm.* **221**, 221 (2017).
- [25] P. K. Schelling, S. R. Phillpot, and P. Keblinski, Comparison of atomic-level simulation methods for computing thermal conductivity, *Phys. Rev. B* **65**, 144306 (2002).
- [26] F. Tong, X. S. Miao, Y. Wu, Z. P. Chen, H. Tong, and X. M. Cheng, Effective method to identify the vacancies in crystalline GeTe, *Appl. Phys. Lett.* **97**, 261904 (2010).
- [27] A. V. Kolobov, J. Tominaga, P. Fons, and T. Uruga, Local structure of crystallized GeTe films, *Appl. Phys. Lett.* **82**, 382 (2003).
- [28] M. Sist, H. Kasai, E. M. J. Hedegaard, and B. B. Iversen, Role of vacancies in the high-temperature pseudodisplacive phase transition in GeTe, *Phys. Rev. B* **97**, 094116 (2018).
- [29] J. Li *et al.*, Simultaneous optimization of carrier concentration and alloy scattering for ultrahigh performance GeTe thermoelectrics, *Adv. Sci.* **4**, 1700341 (2017).

- [30] T. Xing *et al.*, Superior performance and high service stability for GeTe-based thermoelectric compounds, *Natl. Sci. Rev.* **6**, 944 (2019).
- [31] Y. Jin *et al.*, Realizing high thermoelectric performance in GeTe through optimizing Ge vacancies and manipulating Ge precipitates, *ACS Appl. Energy Mater.* **2**, 7594 (2019).
- [32] E. Nshimiyimana *et al.*, Discordant nature of Cd in GeTe enhances phonon scattering and improves band convergence for high thermoelectric performance, *J. Mater. Chem. A* **8**, 1193 (2020).
- [33] Z. Liu *et al.*, Phase-transition temperature suppression to achieve cubic GeTe and high thermoelectric performance by Bi and Mn codoping, *Proc. Natl Acad. Sci. USA* **115**, 5332 (2018).
- [34] P. G. Klemens, Effect of point defects on the decay of the longitudinal optical mode, *Physica B* **316**, 413 (2002).